Multisensory integration (MSI) by polymodal sensory neurons dictates larval settlement in a brainless cnidarian larva

Sydney Birch*[1], David Plachetzki*[1]

[1]Department of Molecular, Cellular, and Biomedical Sciences; University of New Hampshire; Durham, NH, 03824; USA

Corresponding authors:
Sydney.birch@unh.edu
David.plachetzki@unh.edu

Abstract

Multisensory integration (MSI) combines information from two or more sensory modalities and results in a different response from the individual sensory stimuli. Larvae of sessile marine invertebrates use environmental sensory stimuli to irreversibly settle and metamorphose. It can be expected that with such an important survival decision larvae leverage information from multiple sensory modalities. However, MSI has yet to be deeply investigated in marine larvae that lack complex nervous systems and brains. Here, we examined the settlement response of the actinula larva of the hydrozoan *Ectopleura crocea*, which possess a diffuse nerve net, and found that actinulae utilize MSI during larval settlement. We performed a factorial larval settlement study that revealed larvae are sensitive to photo- chemo- and mechanosensory cues and settle in complex ways to different combinations of cues, indicating MSI. In addition, a developmental transcriptome study revealed peak expression of a comprehensive set of candidate sensory genes at the developmental stage when larvae are competent to settle. Finally, RNA fluorescent *in situ* hybridization studies of candidate sensory genes showed that many of the sensory genes of interest are expressed in the same sensory neuron, suggesting that the process of MSI in *E. crocea* takes place within a sensory neuron and not between specialized neurons or neural regions as in other animals. Our results indicate that MSI plays an important role in mediating the larval settlement decision in *E. crocea* and suggests that this process may be accomplished by integrating different lines of sensory information within a polymodal sensory neuron.

Keywords (7):
Multisensory Integration, Larval Settlement, Cnidaria, Hydrozoa, Sensory Cue, RNAseq, Sensory Cue Hierarchy

Introduction

A distinguishing feature of animals is their exquisite capacity to receive sensory information from the environment and integrate it into behavior. Animals may integrate sensory signals from individual modalities (e.g. vision or taste), or they may perform multisensory integration (MSI), which combines information from more than one modality to elicit behaviors that are distinct from behaviors modulated by a single mode (Stein et al. 2009, 2014). MSI is best understood in bilaterian animals with complex nervous systems that include specialized centers for information processing and exchange (Stein 1998; Otto et al. 2013; Stein et al. 2014; Ghosh et al. 2017; Currier and Nagel 2020). Sensory integration is critically important for sessile marine invertebrates that utilize larvae for dispersal and often, irreversible settlement decisions. Larvae place emphasis on select cues, presumably leading to a hierarchy of sensory cues that determine where settlement occurs (Kingsford et al. 2002; Müller and Leitz 2002; Woodson et al. 2007; Hodin et al. 2018). However, MSI has yet to be demonstrated in marine invertebrate larval settlement, and little is known about the potential for MSI in such organisms that lack complex nervous systems or brains.

Here we describe integrative studies on the sensory biology of settlement in the *Ectopleura crocea* actinula larva, a benthic colonial cnidarian species with a pan-global distribution in temperate coastal regions. Immunohistochemical studies of larval neural network development indicate that *E. crocea* larvae first possess a defined nervous system complete with robust tentacular cnidocytes and sensory neurons by the actinula stage of development. Next, to identify the sensory cues involved in settlement, we performed a factorial larval settlement study that investigated the effects of individual and combined cues (e.g., light, chemical (biofilm), and mechanical/surface texture) corresponding to three prominent sensory modalities. We found strong evidence of MSI during larval settlement where the highest rates of settlement occurred in the presence of all three sensory cues and where the effects of cues changed in the presence or absence of other cues, resulting in a sensory cue hierarchy. Developmental transcriptome studies revealed previously undescribed, deep homological links with bilaterian sensory system development and a peak expression of sensory transduction components for each of the three modalities in actinulae stage larvae. Lastly, RNA Fluorescent *in situ* Hybridization (FISH) studies localize several prominent sensory transcripts including opsin (photosensitivity), PKD2L1, and PKD2L3 (chemosensitivity), and ASIC, piezo, and TRPA (mechanosensitivity) to cnidocytes and their attendant sensory neurons in competent actinulae. Our results demonstrate MSI in the brainless actinula of *E. crocea* and suggest that this capacity is facilitated by the activities of polymodal, chemo-photo-mechanoreceptive sensory neurons with distant ancestry to bilaterian unimodal primary sensory neurons.

Results

Larval nervous systems reach full development by the actinula stage of development

The actinula stage of *E. crocea* possesses morphological and cellular features such as the basal protrusion and tentacles replete with cnidocytes, that are associated with larval settlement

(Yamashita 2003). However, the structure of the nervous system throughout larval development has not been examined. We stained larvae at four developmental stages, including the metamorphosed juvenile polyp stage, using immunohistochemistry (IHC) and confocal microscopy (Fig 1). The state of the nervous system at the earliest stage, the star embryo (Fig 1A), appears granular and undifferentiated, which we interpret as a contiguous assemblage of neural progenitor cells (Rentzsch et al. 2017). The larval nervous system becomes increasingly differentiated as development proceeds from the preactinula (Fig 1B) to the actinula stage (Fig 1C-F), whereupon the tentacles are loaded with neurons and cnidocytes (Fig 1E-F). Additionally, the basal protrusion, the structure that comes into contact with the substrate during settlement, contains a concentrated ring of neural cells (Fig 1C). These data are consistent with the actinula stage being the competent stage for settlement and suggest that actinulae have the capacity to integrate sensory information using the tentacles and the basal protrusion.

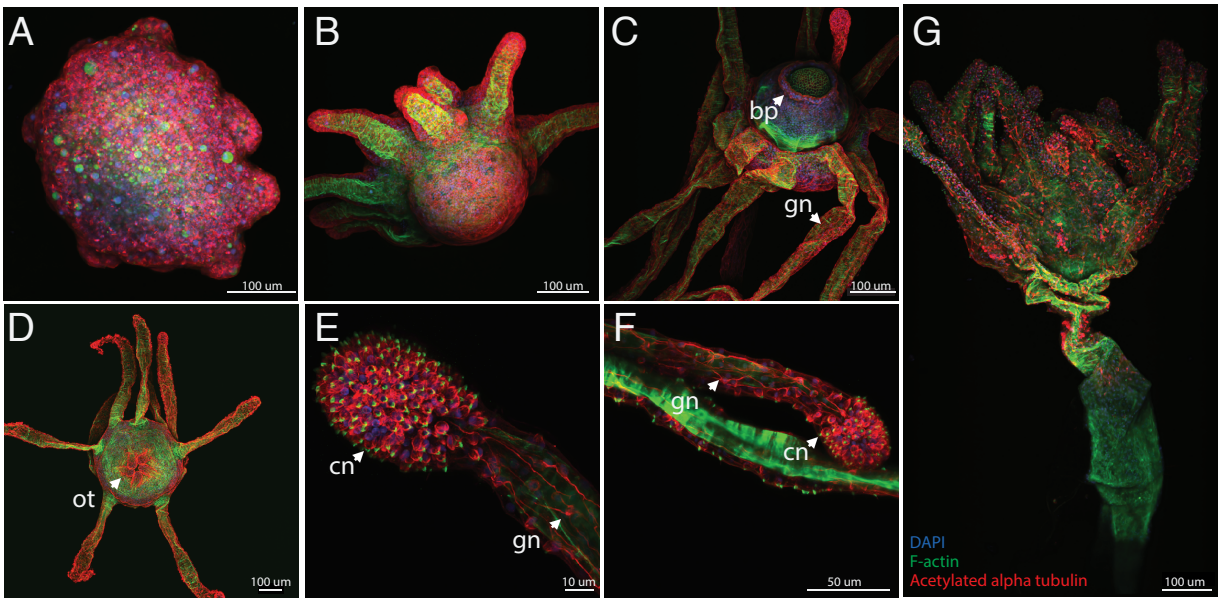

Figure 1. Nervous system development of *Ectopleura crocea* actinulae larvae
A-G Immunohistochemistry (IHC) staining of four developmental stages of *E. crocea* larvae where red staining corresponds to acetylated alpha-tubulin expression in neurons, green staining corresponds to contractile F-actin in muscles and stereocilia, and blue staining corresponds to DNA in nuclei. (**A**) Stage 1, star embryo. (**B**) Stage 2, preactinula. (**C**) The aboral end of a Stage 3-4 actinula larva. The white arrow points to the basal protrusion (bp) which attaches to the substrate during settlement. Other arrow indicates ganglion neurons (gn) in the tentacles. (**D**) Oral end of an actinula larva at stage 3-4. The white arrow is pointing to the developing oral tentacles (ot). (**E-F**) High magnification of stage 3-4 actinula tentacles. An abundance of cnidocytes (cn), indicated by the white arrows, at the tips of the tentacles. Additionally, ganglion neurons (gn) extend down the tentacles and connect to the actinular nerve net. (**G**) A metamorphosed juvenile polyp.

Differences in the sensory environment impact larval settlement

Next, we investigated the sensory information actinula integrate in support of the settlement decision. We performed a factorial settlement study (Fig 2) assessing the impact of

photosensory, chemosensory, and mechanosensory cues on larval settlement, which we analyzed using a three-way analysis of variance (ANOVA). Our experiment included 10 blocks (replicates) where each block had 28 treatments of all possible combinations of cues and examined a total of 2,800 individual actinula larvae (Fig 2A). While the blocking variable, which was the experimental day, did not influence the response, larval settlement did increase as the season progressed, similar to Yamashita et al (2003) (Fig S2). All three individual sensory cues significantly impacted settlement when assessed individually (light, p=0.0482; chemical, p=<2e-16; mechanical, p=<2e-16; Fig 2B-D; Table S1). Specifically, the rate of larval settlement increased significantly in the presence of light compared to darkness (p=0.0482; Fig 2B), and in the presence of the chemical cue compared to its absence (p=<2e-16; Fig 2C) but decreased in the presence of a mechanical cue (p=<2e-16; Fig 2D), when no other cues were present.

The effect of photosensory cues on settlement (wavelengths of light) was investigated in the light-only treatment (Fig 2E) using contrast analyses, since this treatment included additional dimensions compared to chemical and mechanical cues (e.g., presence/absence of light, three wavelengths, and two intensities, totaling 7 light conditions; Fig 2A). Settlement increased in the presence of light compared to darkness (p=0.0027; Fig 2E and Fig 2B, Table S3). In addition, significantly higher settlement occurred in green wavelengths of light (p=0.00167; Fig 2E), whereas significantly lower settlement occurred in red wavelengths (p=0.01137; Fig 2E), compared to the other two wavelengths. No significant interaction between light intensity and light wavelength was detected.

Multisensory integration and a sensory cue hierarchy determine settlement in actinulae

Multisensory integration is detected by examining statistical interactions between different sensory conditions (Stein et al. 2009). Here we examined interactions between sensory cues using a three-way ANOVA and contrasts based on our experimental approach (Fig 2A; Table S4). No interaction between light and chemical cues were identified across experiments (p=0.33; 70 experiments total; Fig 2F and Fig 2I). Similarly, no significant interaction (p=0.89) was observed between light and mechanical cues (Fig 2G and Fig 2J). Conversely, chemical and mechanical cues displayed a significant positive interaction (p=<2e-16; Fig 2K). Alone, chemosensory cues were a strong determinant of larval settlement. However, in the combined presence of the mechanical cue, settlement rates were significantly enhanced, indicating an inversion in the sign of the mechanical cue in the presence of the chemical cue (biofilm). Recall that when the chemical cue was absent, the mechanical cue had a significant negative influence on settlement (p=<2e-16; Fig 2K).

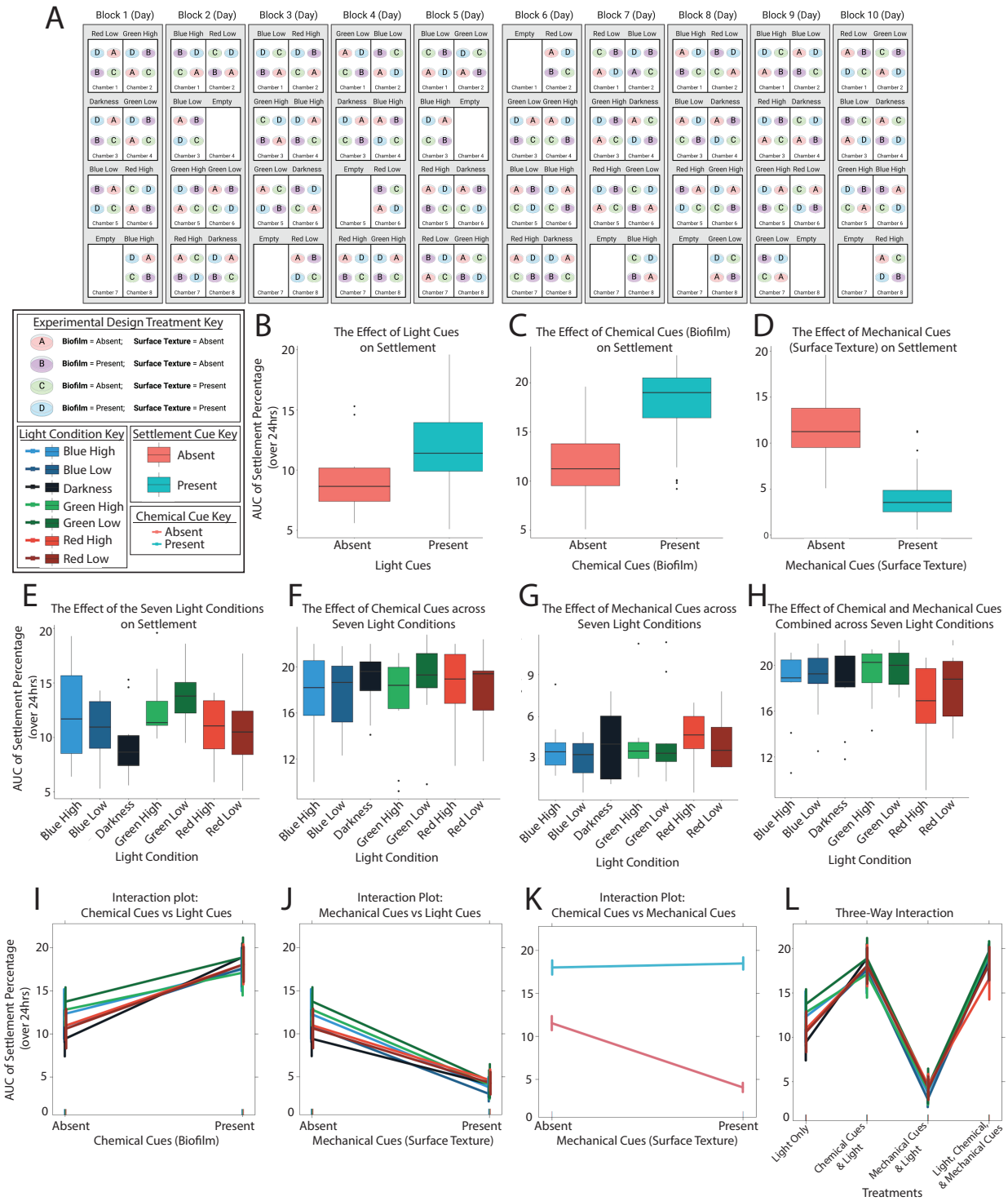

Figure 2. Settlement responses of actinula larvae to three sensory cues (**A**) Cartoon depiction of the larval settlement experimental design: 7x2x2 Split-plot Randomized Complete Block Design (RCBD) with 10 replicates. The block represents an experimental day which is also a replicate. We included all four combinations of presence and absence of biofilm and surface texture which are depicted as A-D treatments, where each biofilm and texture combination was exposed to all 7 light conditions in a single replicate. (**B**) The individual effect of light cues on settlement. Larval settlement is significantly higher (p=0.0027) in the presence of a light cue compared to the absence of a light cue (darkness). (**C**) The individual effect of chemical cues

(biofilm) on settlement. Larval settlement is significantly higher (p=<2e-16) in the presence of a chemical cue compared to the absence of one. (**D**) The individual effect of mechanical cues (surface texture) on settlement. Larval settlement is significantly lower (p=<2e-16) in the presence of a mechanical cue compared to the absence of one. (**E**) The effect of the seven light conditions on settlement. Larval settlement was significantly lower in darkness (p=0.00272) and in red wavelengths of light (p=0.01137) and significantly higher in green wavelengths of light(p=0.00167). (**F**) The effect of chemical cues (biofilm) across the seven light conditions. There were no significant differences in settlement in any wavelength of light (blue p=0.51; green p=0.60; red p=0.88) in the presence of a chemical cue. (**G**) The effect of mechanical cues (surface texture) across the seven light conditions. There were no significant differences in settlement in any wavelength of light in the presence of a mechanical cue (blue p=0.99; green p=0.79; red p=0.79). (**H**) The effect of chemical and mechanical cues combined across the seven light conditions. There was a significant increase in settlement in the presence of green wavelengths of light (p=0.02) and significantly lower settlement in red wavelengths of light (p=0.003). (**I**) The interaction of chemical cues and light cues. There was no significant interaction between these two cues (p=0.33). (**J**) The interaction between mechanical cues and light cues. There was no significant interaction between these two cues (p= 0.89). (**K**) The interaction between chemical and mechanical cues. There was a significant interaction between these two cues (p=<2e-16) with an additive effect in the presence of both cues. (**L**) The three-way interaction of chemical, mechanical, and light cues. Treatment A is the light cues only treatment, treatment B is light and chemical cues, treatment C is light and mechanical cues, and treatment D is all three cues. There is a significant three-way interaction (p=0.02).

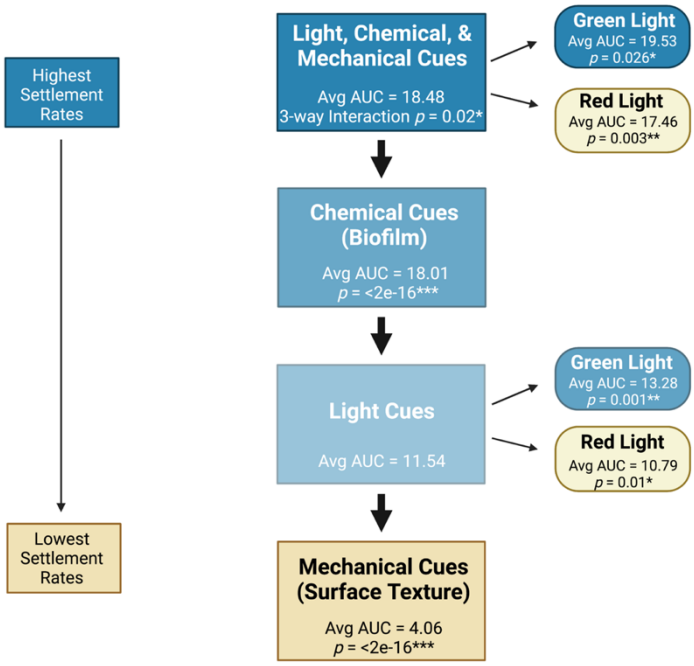

Figure 3. Sensory cue hierarchy of larval settlement in actinula larvae
The highest rates in settlement occur in the presence of all three cues, where significantly higher settlement rates occurred in the presence of green light, and significantly lower settlement rates occurred in the presence of red light. Following the combination of all three cues is the second tier composed of chemical cues which significantly increases larval settlement rates, but not to the same magnitude as having all three cues present. Light did not interact with chemical cues, leading to the lack of a light hierarchy in this second tier. The third tier is the light cues only treatment, where the highest rates of settlement occur in green light and the lowest rates occur in red light. Lastly, is the Mechanical cue tier which significantly decreased settlement rates. Additionally, the scale of color indicates the strength of a cue (darker colors indicate stronger influence).

Finally, the three-way interaction between photo-, chemo-, and mechanosensory cues from the ANOVA is also significant (p=0.022) and indicates MSI by enhancement (Stein et al. 2009). The multisensory response has a significantly higher mean than the largest unisensory response (chemosensory) and the chemo-mechanical response in the absence of light (Fig 3 and Fig. 2L). Among the three-way interaction, larval settlement was significantly lower in darkness when chemical and mechanical cues were present (p=0.03; Fig 2H and L). Additionally, the rate of settlement is significantly higher in green light in the presence of chemical and mechanical cues (p=0.026), and significantly lower in red light (p=0.003; Fig 2H and L). This interaction can be seen in Fig 2L, which shows that green light at both intensities induce higher settlement rates under chemical, and mechanical cues, and lower settlement rates occur in red light. Together, the Area under curve (AUC) data for the different combinations of cues depict a sensory cue

214 hierarchy (Fig 3) where the highest rates of settlement occur in the presence of light, chemical,
215 and mechanical cues.
216
217 **Sensory gene expression peaks in competent larvae and diminishes during and after**
218 **metamorphosis**
219
220 We performed a comparative transcriptome study on six developmental stages of *E. crocea,*
221 from star embryo to metamorphosed juvenile polyp, to assess genetic correlates of the
222 observed sensory response. Illumina Hi-seq sequencing resulted in an average of 38 million
223 reads per replicate, with six replicates for each of the six developmental stages. We first used
224 orthology analyses to place assembled *E. crocea* transcripts into orthogroups that included
225 sequence data from a selection of metazoan genomes including human. We then used the
226 Gene Set Enrichment Analysis (GSEA) database (Subramanian et al. 2005; Liberzon et al. 2011,
227 2015) and EdgeR to identify transcripts with significant differences in expression between any
228 developmental stage that were present in three gene sets: Sensory perception of light stimulus
229 (212 genes in gene set; Fig 4A), Sensory perception of chemical stimulus (501 genes in gene set;
230 Fig 4B), and sensory perception of mechanical stimulus (164 genes in gene set; Fig 4C).
231
232 Gene expression for both the photo- and mechanosensory gene sets share similarities across
233 larval development (Fig 4). First, genes involved in neurogenesis, cellular morphogenesis, and
234 sensory cell type specification show maximum expression early and peak at stage 2 of
235 development (preactinula). Examples of these for the sensory perception of light stimulus gene
236 set include *E. crocea* homologs of SEMA5B (axonal guidance), homologs of CRX, VSX1, VSX2,
237 and RAX2 (transcription factors, photoreceptor specification), NRL2E3 (transcription factor, rod
238 specification), RRH (opsin, detection of light) and others (Fig 4A). A similar pattern is observed
239 for the perception of mechanical stimuli gene set and include *E. crocea* homologs of MYH14
240 (cell shape and cytokinesis), EPS8L2 (stereocilia maintenance), DRGX (nociceptive sensory
241 neuron development) and others (Fig 4C).
242
243 Next, a later pulse of gene expression associated with sensory physiology, cellular structure and
244 morphogenesis, and another round of sensory cell type specification characterizes both gene
245 sets. Examples of these later expressed transcripts for the perception of light stimuli gene set
246 include homologs of GUCY2F and RRH (phototransduction), MYO3B (photoreceptor cell
247 maintenance), ADGRV1 (development of hearing and vision), CNNM4 (retinal function), WHRN
248 (periciliary membrane complex maintenance), and POU4F2 (retinal ganglion cell development).
249 Genes that peak at stages 3 and 4 (actinula) from the perception of mechanical stimuli gene set
250 include CLIC5 (stereocilia formation), MYO3B (cochlear hair bundle morphogenesis), POU4F2
251 (terminal differentiation of hair cells), SLC25A5 (motor protein, modulates auditory stimuli),

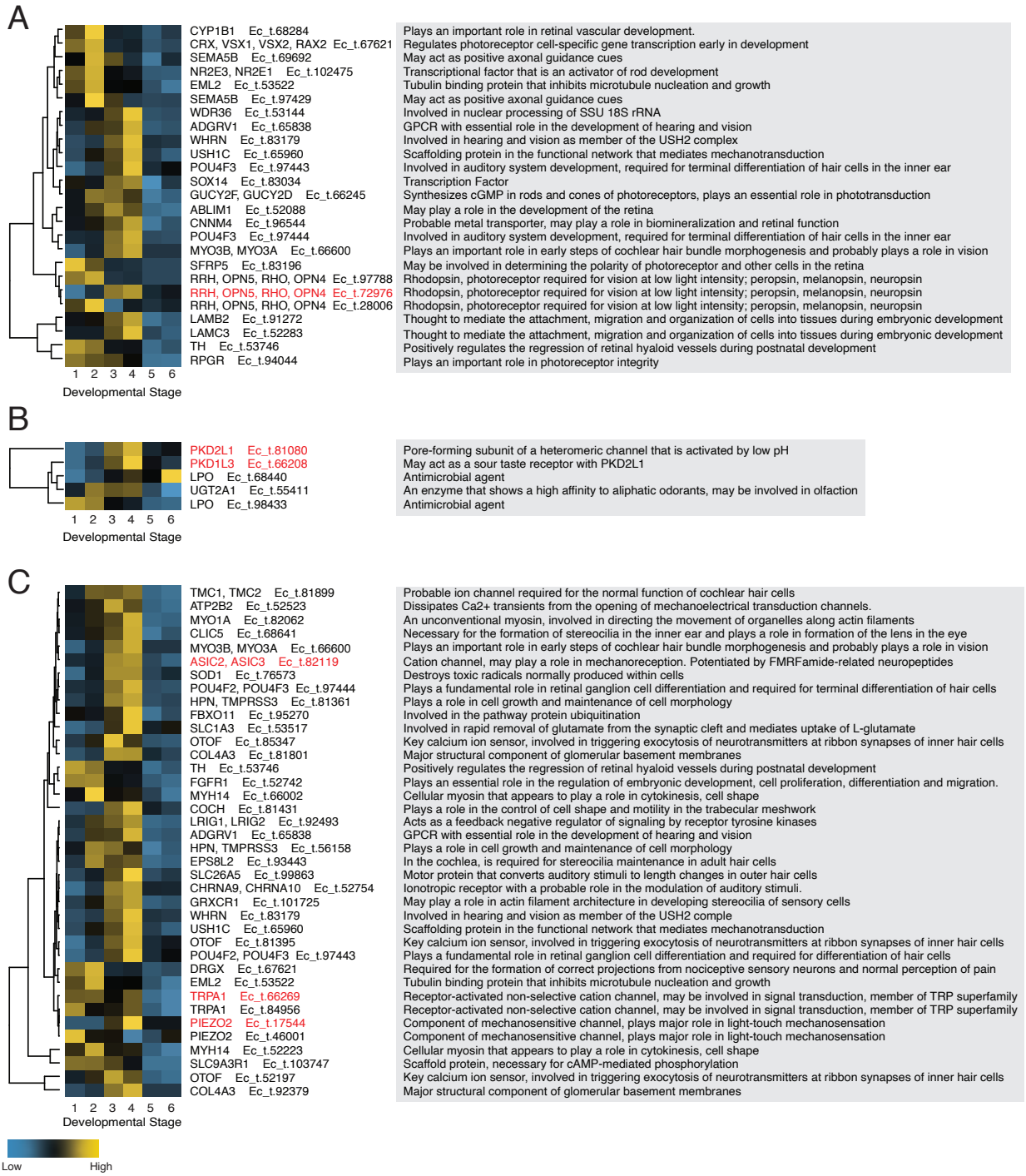

Figure 4. Gene expression over development in actinulae larvae for three sensory gene sets
Heatmaps of significantly differentially expressed genes over development for the following three gene sets: (**A**) sensory perception of light stimulus; (**B**) sensory perception of chemical stimulus; and (**C**) sensory perception of mechanical stimulus. High expression is signified by yellow and low expression is light blue. The grey panels to the right contain abbreviated descriptions of gene functions from UniProt. The transcripts highlighted in red are the transcripts used to make RNA Fluorescent *in situ* hybridization probes. Developmental stages: 1 *star embryo*, 2 *preactinula*, 3 *young actinula*, 4 *actinula in nematocyte-printing stage*, 5 *settled (attached) actinula*, 6 *metamorphosed juvenile polyp*.

262 ASIC2-3 (mechanoreception, potentiated by FMRFamide-related peptides), TRPA1
263 (mechanoreceptor transduction channel), and PIEZO2 (component of a mechanosensitive
264 channel). Finally, transcript expression for both gene sets strongly diminishes at stages 5 and 6,
265 which correspond to metamorphosis and the establishment of the primary polyp. This drop-off
266 in expression is specific to the sensory gene sets used to interrogate our data and is not a
267 general feature of our transcriptome data (Fig S3). It is noteworthy that many of the transcripts
268 that show differential expression in development for either the photo- or mechanosensory
269 gene sets have shared functions in both.
270
271 Similar analyses for the sensory perception of chemical stimulus gene set indicate a markedly
272 different trend as few developmentally differentially expressed transcripts were recovered for
273 this set. However, they do indicate strong stage 4 (actinula) differential expression of homologs
274 of both PKD2L1 and PKD1L3, which dimerize and facilitate sour taste perception in mammals.
275
276 **RNA Fluorescent *in situ* hybridizations reveal evidence for polymodal sensory cells**
277
278 Our studies of larval nervous system development, settlement behavior, and developmental
279 transcriptomics portray an inflection of sensory capacity at stage 4 when actinulae are
280 competent to settle. In order to elucidate the cell types associated with enhanced sensory
281 capacity, and potential cellular partitioning among the different sensory modalities, we
282 conducted fluorescent *in situ* hybridization (FISH) using RNA probes against selected, highly
283 differentiated sensory transcripts (Fig 4) in stage 4 *E. crocea* actinulae. Our targeted transcripts
284 include opsin (Ec_t.72976, photoreception), Piezo and TRPA1 (Ec_t.17544 and Ec_t.66269
285 respectively, mechanotransduction), and ASIC, PKD2L1, and PKD2L3 (Ec_t.82119, Ec_t.81080
286 and Ec_t.66208 respectively, chemotransduction). We examined the cellular and spatial
287 expression of these transcripts using the opsin probe as a reference present in all FISH
288 experiments (Fig 5). Confocal optical sections (0.2 μm) indicate colocalization between most of
289 the transcripts examined. *E. crocea* transcripts corresponding to opsin, and PKD2L1 strongly
290 colocalize to sensory neurons associated with cnidocytes with weaker expression of Piezo in
291 these cells. Conversely, Piezo is strongly expressed in cnidocytes, with weaker expression of
292 both opsin and PKD2L1 in cnidocytes (Fig 5 A-G). Opsin and PKD1L3 are also specifically co-
293 expressed in sensory neurons with broader expression of ASIC in both sensory neurons and
294 cnidocytes (Fig 5 H-N). Finally, opsin and PKD2L1 show some co-expression with TRPA, but most
295 TRPA expression is observed in cnidocytes to the exclusion of opsin and PKD2L1, which are
296 expressed primarily in sensory neurons (Fig 5 O-U). Our results were confirmed by quantifying
297 colocalization using Manders' Overlap (Fig S4).
298

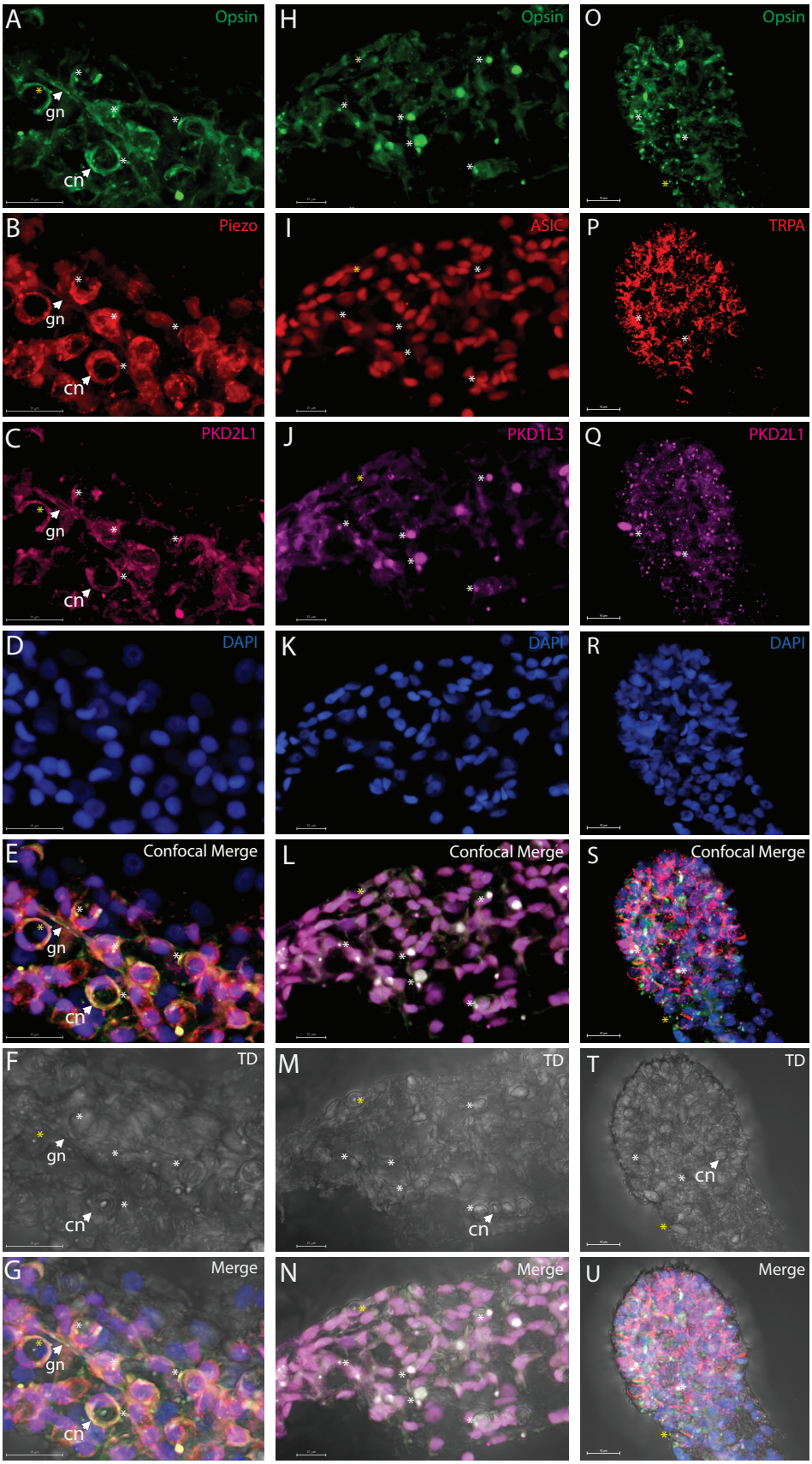
A
Opsin
gn
cn
H
Opsin
O
Opsin
B
Piezo
gn
cn
I
ASIC
P
TRPA
C
PKD2L1
gn
cn
J
PKD1L3
Q
PKD2L1
D
DAPI
K
DAPI
R
DAPI
E
Confocal Merge
gn
cn
L
Confocal Merge
S
Confocal Merge
F
TD
gn
cn
M
TD
cn
T
TD
cn
G
Merge
gn
cn
N
Merge
U
Merge

299

Figure 5. RNA fluorescent *in-situ* hybridizations (FISH) of sensory transcripts in actinulae tentacles (**A-G**) Same tissue. (**A**) Opsin in green, (**B**) Piezo in red, (**C**) PKD2L1 in cyan, and (**D**) DAPI in blue. **(E)** The merge of all confocal channels separated from the transmitted light (TD) channel (**F**). (**G**) The merge of all five channels. For all images in the figure, the white asterisks indicate co-localization of the sensory transcripts in cnidocytes (cn) and sensory neurons (sn). Additionally, arrows point to ganglion neurons (gn) which are synapsed on to by sensory neurons and cnidocytes. Yellow asterisks indicate transcripts localizing to the cnidocil. (**H-N**) Same tissue. (**H**) Opsin in green, (**I**) ASIC in red, (**J**) PKD1L3 in cyan, and (**K**) DAPI in blue. (**L**) The confocal merge separated from the (**M**) TD channel. (**N**) The merge of all five channels. (**O-U**) Same tissue. (**O**) Opsin in green, (**P**) TRPA in red, (**Q**) PKD2L1 in cyan, and (**R**) DAPI in blue. (**S**) Merge of the confocal channel separated from (**T**) the TD channel. (**U**) The merge of all five channels. All scale bars are 10um.

Conclusion

Understanding how cnidarians integrate sensory information from the environment is critical to understanding the ecological processes that dictate benthic community composition. At the same time, uncovering the genetic determinants of cnidarian sensory behavior can illuminate the deep evolutionary histories of the animal senses and provide clues on their early functions. We show that brainless actinula larvae use multisensory integration (MSI) during the larval settlement decision that incorporates information processing from the light, chemical and mechanical senses. MSI is usually portrayed as a process involving information flow between higher-level brain centers (Stein 1998; Otto et al. 2013; Stein et al. 2014; Ghosh et al. 2017; Currier and Nagel 2020), however, our results indicate that MSI is possible at the level of the cell and may have been a prominent feature of the organismal biology of metazoans prior to the evolution of complex brains (Swafford and Oakley 2018).

Methods

Field collection of *E. crocea* Colonies

Larva were obtained by collecting adult *E. crocea* colonies at the UNH Coastal Marine Lab (CML) pier in New Castle, NH in June and July 2020. Colonies were transported to UNH in unfiltered sea water immediately after collection. The colonies were cultured and maintained according to Mackie (1966) where colonies were placed in large glass bowls for predator and dirt removal. Once cleaned, colonies were moved to new bowls filled with unfiltered sea water and were placed in an incubator with an aeration stone connected to a bubbler at a 12/12 L:D cycle at 18°C. Colonies were undisturbed overnight to allow spawning and actinula release. Actinula were identified and collected the following day for settlement experiments or for staining.

Immunohistochemistry and Confocal Microcopy

Immunohistochemistry was performed on four developmental stages: embryos, pre-actinulae, actinula larvae, and juvenile polyps, which were obtained as described above. Samples were fixed overnight at 4°C in 4% paraformaldehyde (Sigma) in PBST. We followed the protocol from Plachetzki et al. (2012) with minor alterations for staining. Samples were washed five times with 5 minute incubations in PBST (3.2 mM Na2HPO4, 0.5 mM KH2PO4, 1.3 mM KCl, 135 mM NaCl, 0.1% Tween 20, pH 7.4) and blocked for 2 h in PBST + 20% normal goat serum (NGS; Sigma) at room temperature. Samples were then incubated with primary antibody, anti-

345 acetylated α tubulin (1:500; Sigma), in blocking solution over night at 4°C. Following the
346 primary antibody, samples were washed five times with 5 min incubations in PBST and blocked
347 as before. Samples were then incubated with the secondary antibody, Cy2-conjugated anti
348 mouse IgG (1:1000; Jackson), and blocking reagent overnight at 4°C. Samples were then washed
349 five times with 5 min incubations in PBST. Afterwards, a solution containing Alexa Fluor 488-
350 labeled phalloidin stock (1:40; Invitrogen) in PBST was added for 1 h. Samples were then
351 washed five times with 10 min incubations and were then mounted in ProLong Antifade
352 Mountant with DAPI (ThermoFisher). Samples were imaged on the UNH Nikon A1R HD confocal
353 Microscope.
354
355 **Larval Settlement Study Experimental Design and Materials**
356 The larval settlement study was designed as a 7x2x2 split-plot Randomized Complete Block
357 Design (RCBD) with 10 blocks, Fig 1A. The blocking variable was the experimental day that
358 replicates were performed on where larvae in one block were from colonies collected at the
359 same time and location the day prior to the experiment. The purpose of the blocking variable
360 was to account for environmental variation between colonies and days across the study, and
361 each block contained all 28 treatments. An experimental unit was a single petri dish that
362 contained 10 actinula larvae, this allowed us to use the area under the curve (AUC) as our
363 response variable. The three treatment factors were the sensory cues of interest which
364 included seven levels of light conditions, two levels of chemosensitive treatments, and two
365 levels of mechanosensitive treatments. Replicates were performed in four hand-made light
366 boxes where each light box had two chambers (described below). The first randomization of the
367 split-plot design, which was applied at the chamber level, were the seven light conditions
368 described in Table 1. The second randomization was comprised of the chemical and mechanical
369 cues and were applied at the petri-dish level in a factorial presence/absence structure and can
370 be seen in Table 2.
371
372 Table 1. The seven levels of the light condition factor with their corresponding measurements

Light Conditions in Study	Wavelength	Intensity
Red Light, High Intensity	630nm	10 µmol m-2 s-1
Red Light, Low Intensity	630nm	5 µmol m-2 s-1
Green Light, High Intensity	520 nm	10 µmol m-2 s-1
Green Light, Low Intensity	520 nm	5 µmol m-2 s-1
Blue Light, High Intensity	460nm	10 µmol m-2 s-1
Blue Light, Low Intensity	460nm	5 µmol m-2 s-1
Darkness	0nm	0 µmol m-2 s-1

373
374 Table 2. Factorial Structure of Chemical and Mechanical Cue Dish Treatments

	Chemical Cue Absent	**Chemical Cue Present**
Mechanical Cue Absent	Dish Treatment A	Dish Treatment B
Mechanical Cue Present	Dish Treatment C	Dish Treatment D

375
376 Prior to settlement experiments, four five-sided light boxes were created with black opaque
377 acrylic (Acrylite; Extruded 9M001) with a thickness of 0.177 inch (in) and 16in x 12in x 12in

dimensions with two centered, circular holes with diameters of 85mm cut out of the top. An additional piece of acrylic with the same thickness with 12in x 12in dimensions was placed in the center of the box to create two separate chambers. Super Bright LEDs heatless lights (part #: WRLFA-RGB6W-60) were placed in the cutout holes which allowed control of four different light intensity settings for the wavelengths red (630 nm), green (520 nm), and blue (460 nm). Light intensity was measured using an LI-1000 DataLogger. For replicability the boxes were placed in the same position for each replicate. The positions of petri-dishes were also marked at high and low intensities for each wavelength in each chamber for replicability, Fig S1B.

To obtain chemical cues, we allowed petri-dishes to generate biofilms by placing dishes in mesh dive bags and attached them to the UNH CML pier for 1 week at a depth of 1.5 m (Lee et al. 2008, 2014). Colonized dishes were then transported to the laboratory in seawater collected at the site and were used in settlement studies and for biofilm sequencing (Corcoll et al. 2017). To obtain mechanical stimuli, petri-dishes were scratched by 36-Grit Ceramic Alumina Sandpaper (Lowes; Model #: 9150-052) in a circular motion on the outer part of the dish, then with three scratches, non-overlapping, going from one side to the other in the center of the dish to ensure full coverage. Dishes were then rinsed twice, once with DI water to remove any plastic shavings, and then a second time with sea water immediately prior of use in a replicate to ensure removal of plastic shavings.

Larval Settlement Study

Larva were obtained by collecting adult *E. crocea* colonies at the UNH CML pier in New Castle, NH in June and July 2020. Colonies were cultured and maintained according to Mackie (1966) as described above. Colonies of *E. crocea* were undisturbed overnight (12-15 hours) to allow spawning and actinula release. The following day, larvae at the actinula stage were collected and placed in 100mm x 15mm plastic petri dishes (Thermo Scientific) where each petri dish contained 10 larvae and the dish treatments corresponded to the predetermined randomized dish conditions for the 28 experimental treatments. Larvae were identified under a microscope following Yamashita et al. (2003) where we sought out young actinula with stiff tentacles, small and circular bodies, and short aboral poles.

One block (replicate) of all 28 treatment conditions began once larvae were collected at the actinula stage where start times were staggered by chamber which had four petri dishes with a total of 40 larvae. Dishes from the four chemical and mechanical treatment conditions were placed at the appropriate positions and wavelength and light intensity were adjusted according to the predetermined randomized treatment conditions per chamber. Metamorphic stages were recorded at the following time points: 0 hours (hrs), 2hrs, 4hrs, 6hrs, 8hrs, 12hrs, and 24hrs. At each time point, dishes were taken out of the light box and placed under a microscope where each individual larva was observed and quantified based on their metamorphic stage (detailed below). Immediately following quantification, the replicate dish was placed back into the light box until the next time point for quantification, this procedure was performed for each of the 28 dishes at each time point.

421 Larval quantification was assessed on a presence/absence metamorphosis scale with three
422 levels. A 0 signified larvae were still in the actinula phase and had not metamorphosed or
423 settled, a 1 indicated that larvae had settled (attached to the substrate but had not completed
424 metamorphosis), and a 2 signified that larvae had completed metamorphosis into a juvenile
425 polyp. At each time point, we counted and recorded the total number of larvae for each
426 condition under the scale. From this information, we then calculated the area under the curve
427 using the settlement percentages at each time point, which combined the number of settled
428 and metamorphosed larvae (# of Settled + # of Metamorphosed/total # of larvae in dish). The
429 following equation was used to calculate the area under the curve (AUC) which was used as the
430 response variable in statistical analyses (Mohapatra et al, 2014; Shaner, 1977):
431
432 $$\text{AUC} = \sum_{i=1}^{n}[(y_i + y_{i+1})/2] * [t_{i+1} - t_i]$$
433
434 Where y_i is the proportion of settled and metamorphosed larvae at the ith time point; t_i is the
435 timepoint in hours where larvae were observed, and *n* is the total number of observations per
436 petri-dish in a replicate. Normally distributed data were compared statistically by a split-plot
437 RCBD three-way analysis of variance (ANOVA) and with orthogonal contrasts in the R
438 environment.
439
440 **Library preparation, sequencing and read processing**
441 Colonies of *E. crocea* were collected at the UNH CML pier in May and June 2019. Colonies were
442 maintained and larva were obtained as previously mentioned above. We collected six replicates
443 of the six developmental stages: embryos, pre-actinula, actinula (younger), settling actinula
444 (older), settled actinula, and metamorphosed juvenile polyps (Yamashita 2003), where each
445 stage had a total of 125 larva collected. Samples were stored in RNA*later* (Thermo Fisher
446 Scientific) in -20°C until total RNA was extracted using the PureLink RNA Mini Kit (Thermo Fisher
447 Scientific; Cat no. 12183018A) according to the manufacturer's instructions and quantified
448 using NanoDrop (Thermo Scientific). Libraries were created using 1000ng of total RNA with the
449 NEBNext Ultra 2 Directional RNA Library Kit following the Poly(A) mRNA Magnetic Isolation
450 module (NEB #E7490). Libraries were sent to Novogene for Illumina Hi-Seq. After sequencing,
451 reads were processed using custom python scripts which executed FastQC and selected the
452 highest quality replicate for each of the 6 stages. It then concatenated the highest quality
453 replicate for each of the 6 stages to generate representative R1 and R2 read files to be used in
454 *de novo* transcriptome assembly. The Oyster River Protocol (ORP) was used as the assembler
455 which performs read trimming, read normalization, read error correction, and generates an
456 assembly using a multi-kmer and multi-assembler approach and then merges those assemblies
457 into one final high-quality assembly (MacManes 2018). The ORP also produced quality metrics
458 from TransRate and BUSCO.
459
460 **Gene expression analysis**
461 To prepare for gene expression analyses performed later in the workflow, two sub-steps were
462 completed as depicted in Fig S6, an overview of the transcriptome workflow. First, the program
463 Salmon was executed to quantify transcripts in the linux environment (Patro et al., 2017). Next,
464 EdgeR was implemented in the R environment to identify significant differential gene

465 expression between pair-wise comparisons of the six developmental stages (Chen et al. 2020).
466 Count data was reduced by requiring transcripts to have 10 counts in a library to be considered
467 expressed and were filtered by counts-per-million (CPM)(Chen et al. 2020). The
468 calcNormFactors function was used to normalize library sizes which used a trimmed mean of M-
469 values (TMM) method. To estimate dispersion, a quantile-adjusted conditional maximum
470 likelihood (qCML) method was employed. Differentially expressed genes (DEGs) were identified
471 at a p-value of 0.05 and results from each comparison was exported to the terminal and
472 included the transcript header, logFC, logCPM, PValue, and FDR which was used in a later step.
473
474 TransDecoder was then implemented to translate the assembly from nucleotide space into
475 protein space. To reduce the amount of duplicate protein models, we ran cd-hit on the actinula
476 protein FASTA. The reduced actinula FASTA was then used in OrthoFinder along with the
477 following taxa from publicly available data on NCBI: *Homo sapiens*, *Drosophila*, *Hydra*,
478 *Hydractinia* (adult and larval forms), and *Nematostella*.
479
480 While OrthoFinder was running, we obtained sensory gene sets from the Gene Set Enrichment
481 Analysis (GSEA) created by the Broad Institute and UC San Diego (Subramanian et al. 2005;
482 Liberzon et al. 2011, 2015). We selected the following three gene sets:
483 GO_Sensory_Percep_Of_Light_Stimulus, GO_Sensory_Perception_of_Chemical_Stimulus, and
484 GO_Sensory_Perception_of_Mechanical_Stimulus. We then imported the Entrez IDs, gene
485 symbols, and descriptions of the members in the gene sets as a CSV file into the terminal. Using
486 custom made python scripts we reformatted the gene set information and searched the Entrez
487 IDs using the Bio.Entrez module in python to obtain the protein sequences for each gene across
488 the three gene sets.
489
490 Our human protein sequences used in OrthoFinder contained altered headers, therefore we
491 performed three BLASTp searches on our human protein sequences using the genes from the
492 sensory gene sets as queries. The search allowed one target sequence result at an e-value of
493 0.00001. The output from the three searches included the official NCBI headers and the
494 corresponding altered header used in our human protein models. This was used to annotate
495 the altered human protein models used in OrthoFinder with the various sensory genes in the
496 following step. Additionally, we generated another output file that was composed of human
497 sequence IDs from the NCBI database and their corresponding gene symbols.
498
499 To identify actinula transcripts that shared orthogroups with human transcripts of sensory
500 genes, we imported the following results into the R environment to be used in a custom R
501 script: OrthoFinder (orthogroup.tsv file and counts file), the BLAST results with the two human
502 headers (NCBI and the altered headers used in our human protein FASTA), and the file with the
503 NCBI headers and its corresponding gene symbol. This R script then identified and re-labeled
504 the orthogroups that contained the genes from the sensory gene sets with the gene symbols
505 and reported the actinula transcripts that were contained in those orthogroups with the gene
506 symbol labels. The lists of actinula headers with their corresponding gene symbols were
507 exported from R into the terminal and were used with a custom python script and the edgeR

508 output to identify significantly differentially expressed genes within the gene sets. The
509 significant DEGs were then visualized as heatmaps for each gene set in the R environment.
510
511 **RNA Fluorescent *in situ* Hybridization Study**
512 Sequences were identified to make RNA probes for *in situ* hybridizations using the
513 transcriptomic expression data from the developmental transcriptome study. We identified the
514 highest expressed transcripts of key sensory genes from the three sensory gene sets. We then
515 designed RNA-probes for our target sequences using the Stellaris RNA FISH platform (Biosearch
516 Technologies) with the custom probe design service following their recommendations for probe
517 design, sequences can be found in Table S6.
518
519 Actinula larvae were obtained as previously described above. Samples were stained according
520 to the Stellaris FISH protocol with alterations to the protocol. Samples were fixed overnight at
521 4°C in 4% paraformaldehyde (Sigma) in PBS. The following day samples were washed five times
522 with 5 minute incubations in PBST. Samples were then incubated in Prot K (1ug/ul) for 10
523 minutes at room temperature. Immediately following the Prot K incubation, the solution was
524 removed, and samples were incubated in glycine (4ug/ul) for 10 minutes at room temperature
525 to stop the Prot K reaction. Samples were then washed twice with 5 minute incubations in
526 PBST. We then refixed samples in 4% PF for 30 minutes at room temperature. Following
527 refixation, samples were washed five times with 5 minute incubations in PBST. We then
528 transferred samples to 1.5ml microcentrifuge tubes and incubated samples in Wash Buffer A
529 (Catalog# SMF-WA1-60) for 5 minutes at room temperature. We then ran a prehybridization
530 step using the stellaris hybridization buffer (Catalog# SMF-HB1-10) at 37C for 1 hour in a shake
531 'N' bake Hybridization Oven. Following the prehybridization step, we added the hybridization
532 buffer with probes (10ul of each probe for a total of 30ul of probe) to our samples and
533 incubated them at 37C overnight in the dark. The following day, the hybridization buffer with
534 probe solution was removed and samples were incubated in Wash Buffer A at 37C for 30
535 minutes in the dark. Samples were then incubated in Wash buffer B (Catalog# SMF-WB1-20) for
536 5 minutes at room temperature in the dark. We resuspended samples in PBST and mounted
537 them in ProLong Antifade Mountant with DAPI (ThermoFisher). Samples were imaged on the
538 UNH Nikon A1R HD confocal Microscope.
539
540 **References**
541 Chen Y, McCarthy D, Ritchie M, et al (2020) edgeR: differential analysis of sequence read count
542 data User's Guide. R Packag 1–121
543 Corcoll N, Österlund T, Sinclair L, et al (2017) Comparison of four DNA extraction methods for
544 comprehensive assessment of 16S rRNA bacterial diversity in marine biofilms using high-
545 throughput sequencing. FEMS Microbiol Lett 364:1–9.
546 https://doi.org/10.1093/femsle/fnx139
547 Currier TA, Nagel KI (2020) Multisensory control of navigation in the fruit fly. Curr Opin
548 Neurobiol 64:10–16. https://doi.org/10.1016/j.conb.2019.11.017
549 Ghosh DD, Nitabach MN, Zhang Y, Harris G (2017) Multisensory integration in C. elegans. Curr
550 Opin Neurobiol 43:110–118. https://doi.org/10.1016/j.conb.2017.01.005
551 Lee JW, Nam JH, Kim YH, et al (2008) Bacterial communities in the initial stage of marine biofilm

552 formation on artificial surfaces. J Microbiol 46:174–182. https://doi.org/10.1007/s12275-
553 008-0032-3
554 Lee OO, Chung HC, Yang J, et al (2014) Molecular Techniques Revealed Highly Diverse Microbial
555 Communities in Natural Marine Biofilms on Polystyrene Dishes for Invertebrate Larval
556 Settlement. Microb Ecol 68:81–93. https://doi.org/10.1007/s00248-013-0348-3
557 Liberzon A, Birger C, Thorvaldsdóttir H, et al (2015) The Molecular Signatures Database
558 Hallmark Gene Set Collection. Cell Syst 1:417–425.
559 https://doi.org/10.1016/j.cels.2015.12.004
560 Liberzon A, Subramanian A, Pinchback R, et al (2011) Molecular signatures database (MSigDB)
561 3.0. Bioinformatics 27:1739–1740. https://doi.org/10.1093/bioinformatics/btr260
562 Mackie GO (1966) Growth of the hydroid Tubularia in culture. In: The Cnidaria and their
563 Evolution. pp 397–412
564 MacManes MD (2018) The Oyster River Protocol: a multi-assembler and kmer approach for de
565 novo transcriptome assembly. PeerJ 6:e5428. https://doi.org/10.7717/peerj.5428
566 Mohapatra N, Mukherjee A, Suriya Rao A, et al (2014) Comparison of Different Parameters for
567 Evaluation of Partial Resistance to Rice Blast Disease. Am J Exp Agric 4:58–79.
568 https://doi.org/10.9734/ajea/2014/3756
569 Otto TU, Dassy B, Mamassian P (2013) Principles of multisensory behavior. J Neurosci 33:7463–
570 7474. https://doi.org/10.1523/JNEUROSCI.4678-12.2013
571 Patro R, Duggal G, Love MI, et al (2017) Salmon: fast and bias-aware quantification of transcript
572 expression using dual-phase inference. Nat Methods 14:417–419.
573 https://doi.org/10.1038/nmeth.4197.Salmon
574 Plachetzki DC, Fong CR, Oakley TH (2012) Cnidocyte discharge is regulated by light and opsin-
575 mediated phototransduction. BMC Biol 10:. https://doi.org/10.1186/1741-7007-10-17
576 Rentzsch F, Layden M, Manuel M (2017) The cellular and molecular basis of cnidarian
577 neurogenesis. Wiley Interdiscip Rev Dev Biol 6:1–19. https://doi.org/10.1002/wdev.257
578 Shaner G (1977) The Effect of Nitrogen Fertilization on the Expression of Slow-Mildewing
579 Resistance in Knox Wheat. Phytopathology 77:1051. https://doi.org/10.1094/phyto-67-
580 1051
581 Stein BE (1998) Neural mechanisms for synthesizing sensory information and producing
582 adaptive behaviors. Exp Brain Res 123:124–135. https://doi.org/10.1007/s002210050553
583 Stein BE, Stanford TR, Ramachandran R, et al (2009) Challenges in quantifying multisensory
584 integration: Alternative criteria, models, and inverse effectiveness. Exp Brain Res 198:113–
585 126. https://doi.org/10.1007/s00221-009-1880-8
586 Stein BE, Stanford TR, Rowland BA (2014) Development of multisensory integration from the
587 perspective of the individual neuron. Nat Rev Neurosci 15:520–535.
588 https://doi.org/10.1038/nrn3742
589 Subramanian A, Tamayo P, Mootha VK, et al (2005) Gene set enrichment analysis: A knowledge-
590 based approach for interpreting genome-wide expression profiles. Proc Natl Acad Sci U S A
591 102:15545–15550. https://doi.org/10.1073/pnas.0506580102
592 Swafford AJM, Oakley TH (2018) Multimodal sensorimotor system in unicellular zoospores of a
593 fungus. J Exp Biol 221:. https://doi.org/10.1242/jeb.163196
594 Yamashita K (2003) Larval Behavioral, Morphological Changes, and Nematocyte Dynamics
595 During Settlement of Actinulae of Tubularia mesembryanthemum, Allman 1871 (Hydrozoa:

596 Tubulariidae). Biol Bull 204:256–269
597
598